Journal of Chromatography A, 1217 (2010) 1667–1673

Contents lists available at ScienceDirect

Journal of Chromatography A

journal homepage: www.elsevier.com/locate/chroma

Thermal field-flow fractionation and multiangle light scattering of polyvinyl acetate with broad polydispersity and ultrahigh molecular weight microgel components

Dean Lee, S. Kim Ratanathanawongs Williams *

Laboratory for Advanced Separations Technologies, Department of Chemistry and Geochemistry, Colorado School of Mines, 1500 Illinois Street, Golden, CO 80401 1887, USA

ARTICLE INFO

Article history:
Received 5 November 2009
Received in revised form 4 January 2010
Accepted 8 January 2010
Available online 18 January 2010

Keywords:
Thermal field-flow fractionation
Multiangle light scattering
Microgels
Broad polydispersity
Ultrahigh molecular weight polymer
Molecular weight determination

ABSTRACT

The challenging task of characterizing polydisperse polymer mixtures possessing ultrahigh molecular weight (MW) polymers and microgels in organic solvents is addressed with thermal field-flow fractionation (ThFFF) and multiangle light scattering-differential refractive index (MALS-*d*RI) detection. In initial experiments, a 350,000 g/mol poly(methyl methacrylate) (PMMA) standard is used to evaluate the effects of temperature gradient and temperature gradient programming on the measurements. *d*RI baseline fluctuations caused by temperature programming were minimized by using a mobile phase heater to thermostat connecting tubing. ThFFF–MALS-*d*RI is then used to separate and characterize a complex polyvinyl acetate (PVAc) sample containing ultrahigh MW polymers and microgels. The open channel design employed by ThFFF allowed the PVAc sample to be analyzed with minimal sample preparation. Unfiltered PVAc sample showed components with MWs close to 10^9 g/mol and root mean square radius r_{rms} values approaching 400 nm. The same sample, filtered through a 0.5 μm pore-size membrane, yielded a MW that was at least one order of magnitude lower. These results demonstrated that the common practice of prefiltering polymer samples prior to analysis can lead to erroneously low average MWs and polydispersities. The accuracy of MW and r_{rms} calculated using standard light scattering equations developed for small scattering molecules and relatively high wavelengths is also examined.

1. Introduction

Water-borne coatings and adhesives are broad molecular weight distribution (MWD) polymers that are prepared by emulsion polymerization [1]. They contain components with 3-dimensional crosslinked network structure called microgels [2]. These microgels usually have ultrahigh (>10^7 g/mol) MWs and are critical in regulating the rheological properties of the end products [3]. The measurement of molecular weight and size distributions of the microgels is necessary to evaluate and control the performance of the end products. Conventional gravimetric analyses take several days and mainly yield information about the amount of microgels present in a sample [4–8]. The techniques used to characterize microgels fall into three categories: light scattering, imaging, and fractionation. Dynamic light scattering (DLS) is frequently used to obtain hydrodynamic sizes of microgels in the submicrometer range [9–13]. DLS is effective for samples with narrow polydispersity. When dealing with broad polydispersity samples, the measured correlation function is a weighted sum of exponential decay functions contributed by polymers and microgels of individual sizes. Consequently, the extraction of a size distribution from the correlation function is inaccurate (with a bias towards the large size) and subject to artificial errors [14]. Static light scattering has also been used to characterize MW and root mean square (rms) radii of microgels [12,13,15]. Imaging techniques, such as SEM, TEM, and AFM, can give direct size measurement of the "dry state" microgels [9,16,17]. This size is different to that of swollen microgels dispersed in a solvent. As most applications of microgels and microgels-containing polymer mixtures require suspension in an appropriate solvent, the size of the swollen state is important. Moreover, these techniques only show images of a small population of microgels that may not be representative of the entire sample.

The necessity of a separation step for accurate analyses of polydisperse samples has been demonstrated on many occasions, e.g., when utilizing techniques such as MALDI-TOF mass spectrometry and light scattering [18–20]. The main separation methods for polymers include size exclusion chromatography (SEC), packed and capillary hydrodynamic chromatography (HDC), and field-flow fractionation (FFF). Size exclusion chromatography is the most commonly used technique for MWD characterization of polymers. SEC columns fractionate polymer chains according to their hydrodynamic radii and the MWs of the fractionated polymers are

* Corresponding author. Tel.: +1 303 273 3245; fax: +1 303 273 3629.
E-mail address: krwillia@mines.edu (S.K.R. Williams).

0021-9673/$ – see front matter © 2010 Elsevier B.V. All rights reserved.
doi:10.1016/j.chroma.2010.01.035

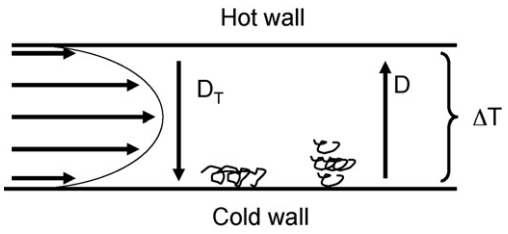

Fig. 1. Normal mode separation mechanism for thermal FFF. Normal diffusion and thermal diffusion are represented by their coefficients, D and D_T, respectively.

estimated from a calibration curve or determined using on-line absolute detectors (differential viscometer and/or light scattering photometer) [21]. SEC, however, often encounters serious problems when it is applied to high and ultrahigh MW samples. The polymers and microgels can be shear-degraded or trapped in the columns and the column exclusion limit can be exceeded leading to underestimated MW values and blockage of the column [22,23]. This behavior has been demonstrated in a direct comparison of high temperature FFF and SEC separation of high MW low density polyethylene [24]. Hence, it is common practice to prefilter polymer samples prior to SEC analysis.

HDC and FFF have higher size limits than SEC and are capable of analyzing samples with submicrometer-size components. Like FFF, HDC utilizes the different flow velocity streamlines of a parabolic flow profile to achieve separation. Unlike FFF, HDC does not employ a field to focus sample components into narrow equilibrium layers. Consequently, HDC exhibits lower molecular weight selectivity (defined as the slope of a log MW versus retention volume plot) [25,26]. FFF possesses the broad dynamic separation range in MWs and the high resolution essential to the successful characterization of polydisperse polymers with ultrahigh MW components [27,28].

The external force applied perpendicular to the separation axis provides the 'field' in FFF [29]. Flow FFF (FlFFF) and thermal FFF (ThFFF) are the two FFF techniques most frequently used for polymer separations. The field employed in FlFFF is a second flow stream (or crossflow) of fluid that is pumped in a perpendicular direction to the axial flow stream. Flow FFF has been predominantly used for aqueous polymer solutions [30–32] because of the difficulty to find suitable membranes for organic solvents. A 10,000 g/mol MW cut-off regenerated cellulose membrane was used to separate >90,000 g/mol PS and styrene–butadiene rubbers in tetrahydrofuran [33]. High temperature FlFFF has been successfully demonstrated for polyolefins with superior performance over SEC for high MW components [24]. However, the high temperatures necessitated the use of a 10 nm pore-size ceramic membrane that was unable to retain polymers below 50,000 g/mol.

Thermal FFF is mostly associated with characterizing polymers in organic solvents [29,34,35] and has been successfully used to fractionate high MW natural rubber and pressure sensitive adhesives [36–40]. The 'field' in ThFFF is the temperature gradient that is applied perpendicular to the separation axis (Fig. 1). The larger the difference in temperature between the ThFFF channel walls or ΔT, the closer the sample components are driven to the cold wall and the slower they move as they are entrained in the slower flowing regions of the parabolic flow profile. This movement of sample towards the wall (usually the cold wall) is represented by thermal diffusion coefficient D_T. The sample concentration build-up at the cold wall leads to the sample's diffusion D away from this wall. At equilibrium, the two opposing transport processes are balanced such that a different average equilibrium distance is attained for each sample component. Separation is achieved because each sample component resides in a different flow velocity streamline and is swept out of the ThFFF channel at a different rate. The ThFFF channel walls are solid and thus the sample loss encountered through the semipermeable flow FFF channel wall is not an issue. ThFFF is mostly used to analyze polymers with molecular weights above 10^4 g/mol but polystyrene as low as 2200 g/mol has been retained in a binary solvent [41].

The dearth of polymer standards, particularly in the ultrahigh MWs region necessitates the on-line coupling of FFF with an absolute MW characterization detector, such as multiangle light scattering (MALS). FlFFF–MALS has been used to characterize numerous bio- and natural polymers [42–44]. However, the use of ThFFF with MALS-differential refractive index (*d*RI) detectors has been limited with a few applications to date involving styrene–acrylonitrile copolymer [45], natural and styrene–butadiene rubber [46,36]. This is likely due to practical concerns such as sufficiently different sample and solvent refractive indices and the effects of ΔT on *d*RI signals.

This study reports the development of ThFFF–MALS-*d*RI for analyzing highly polydispersed samples containing ultrahigh molecular weight polymers and microgels in an organic solvent. Key issues that are examined include the effect of ThFFF temperature gradient programming on the *d*RI signal, the application of the developed method to the characterization of a complex industrial sample, and an estimation of errors in MW and root mean square radius r_{rms} values determined by ThFFF–MALS-*d*RI. Sample recovery and the effectiveness of sample preparation procedure are also important aspects of this work.

2. Experimental

2.1. Materials

Poly(methyl methacrylate) (PMMA) standards were purchased from Polysciences, Inc. (Warrington, PA, USA). The MWs of the standards used in the present study are 30,000 and 350,000 g/mol. The microgel-containing poly(vinyl acetate), coded as PVAc10, was provided by National Starch & Chemical Company (Bridgewater, NJ, USA). HPLC grade acetonitrile is from Mallinckrodt Chemicals (Phillipsburg, VA, USA).

2.2. Sample preparation

The PVAc10 sample, which was received as an emulsion in water, was resuspended in organic solvent using the following procedure. The sample was first washed by adding deionized water and then centrifuged. The PVAc10 was transferred to a vial and dried by blowing air into the vial. The dried sample was resuspended in acetonitrile and heated at 70 °C with gentle stirring for 24 h. The resulting cloudy solution was allowed to sit on the bench overnight to allow undissolved particles to sediment. Work done by National Starch had determined that these particles are mostly poly(vinyl alcohol). The haziness of the PVAc10 supernatant was an indication of the presence of components in the size range of the visible wavelengths. This supernatant with a polymer concentration in the range of 5–8 mg/mL was injected directly into ThFFF separation system for analysis. A second set of samples was prepared by filtering the PVAc10 supernatant through a 0.5 μm pore-size Teflon membrane (Corning, NY, USA). The filtrate was collected in a pre-weighed vial, the solvent was evaporated, and the mass of filtered PVAc10 was thus determined. Different volumes of acetonitrile were added to prepare known concentrations of the filtered sample solution.

2.3. ThFFF system

The ThFFF system consists of a Waters 590 pump, a Valco injector with a 20 μL sample loop, a ThFFF channel, and a combination of Wyatt DAWN F multiangle light scattering (MALS) photometer

and Optilab 903 differential refractometer as the detectors. The ThFFF channel was similar to that available from PostNova Analytics (Salt Lake City, UT, USA) and to that described previously [41] with some modifications. The channel, made from a 127 μm thick Teflon-coated polyimide spacer, had a breadth of 2 cm and tip-to-tip length of 27.4 cm. The cold wall temperature was maintained by a Neslab Coolflow CFT-75 refrigerated recirculator (Thermo Fisher Scientific Inc., Waltham, MA, USA). The hot wall temperature was controlled by the Thermal 1.5 alpha 5 software (PostNova Analytics, Salt Lake City, UT, USA) which also recorded hot and cold wall temperatures as a function of time.

The wavelength of the MALS and differential refractive index (*d*RI) detectors (Wyatt Technologies, Santa Barbara, CA, USA) was 632.8 nm. The MALS detector was calibrated using toluene and normalized with 30,000 g/mol PMMA standard. A 12 μL ultra-sensitive flow cell (P100) was installed in the *d*RI detector.

A 40 cm long fused silica capillary (50 μm i.d.) (Polymicro Technologies, LLC, Phoenix, AZ, USA) was attached to the ThFFF channel to provide a backpressure of 50–100 psi. A mobile phase preheater (Analytical Sales and Services, Inc., Pompton Plains, NJ, USA) was connected between the capillary and the MALS detector. The mobile phase pre-heater was thermostatted at 70 °C in a column oven.

2.4. General ThFFF approach

A constant flow rate of 0.1 mL/min was used in all analyses. The field strength was varied by changing ΔT to achieve an optimum balance between analysis time and resolution. The ΔT program followed the equation [47]

$$\Delta T = \Delta T_0 \frac{t_1 - t_a}{(t - t_a)^p} \quad (1)$$

where ΔT_0 is the initial temperature difference, t_1 is the initial time period where the temperature is held constant (before starting the gradient), t_a is an asymptotic constant that defines the profile of the temperature gradient, t is retention time, and p takes on different optimum values depending on the type of FFF field. During the initial method development stage, a fast ΔT decay was used to rapidly elute sample and thus saves time. A fast ΔT decay also represented an extreme condition in the study of effect of ΔT programming on detector response. In the final sample analysis stage, when higher resolution was desired, a slow ΔT decay was employed. Hence, in Section 3, the ThFFF conditions are referred to as either fast- or slow-decay ΔT.

2.5. MALS-dRI data treatment for MW and size characterization

MALS and *d*RI detectors allowed the estimation of MW and root mean square radius (r_{rms}) of sample components eluting from the ThFFF channel. This estimate is based on the scattered light intensity measured at different angles (θ), the sample concentration (c) obtained from the *d*RI detector, and fitting the data using the well known Zimm, Debye, or Berry [48,49] formalisms. The Berry equation is shown in Eq. (2).

$$\sqrt{\frac{Kc}{R_\theta}} = \sqrt{\frac{1}{M} + \frac{16\pi^2}{3\lambda^2}\frac{1}{M}\langle r_{rms}\rangle^2 \sin^2\left(\frac{\theta}{2}\right)} \quad (2)$$

R_θ is the excess Rayleigh ratio (which is proportional to scattered light intensity), M is weight-average MW (M_w) for polydisperse polymer, $K = 4\pi^2(dn/dc)^2 n_0^2 N_A^{-1}\lambda^{-4}$, dn/dc is specific refractive index increment for the polymer in solution, n_0 is solvent refractive index, N_A is Avogadro's number, and λ is incident wavelength. Eq. (2) incorporates an approximate expression for the form factor [50]

$$P(\theta) = 1 - \left(\frac{16\pi^2}{3\lambda^2}\right)\langle r_{rms}\rangle^2 \sin^2\left(\frac{\theta}{2}\right) \quad (3)$$

that is applicable when the wavelength of incident light is relatively high, the scattering molecule is small, or the scattering angle is small.

The dn/dc of PMMA in acetonitrile and for $\lambda = 633$ nm is 0.136 mL/g. This was obtained by extrapolating dn/dc literature values at 436 and 546 nm using the approximation that dn/dc increases linearly with the inverse of the square of the wavelength of scattering radiation [51]. The dn/dc of PVAc10 was determined on-line using 0.5 μm pore-size filtrate, assuming 100% mass recovery.

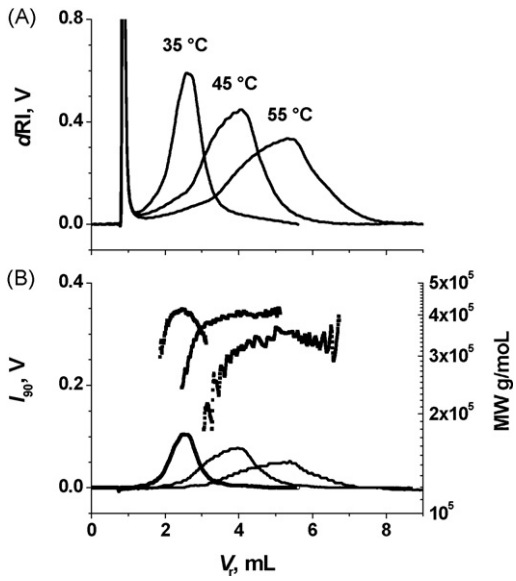

Fig. 2. ThFFF–MALS analysis of PMMA standard (MW = 3.50×10^5 g/mol) at different ΔTs. (A) *d*RI fractograms and (B) I_{90} fractograms and MWs. Concentrations: 2.0 mg/mL at 35 °C; 3.0 mg/mL at 45 and 55 °C.

3. Results and discussion

This study aims to assess the ThFFF/MALS-*d*RI system's ability to obtain useful MW and size information. The effects of different ΔTs (constant and programmed) were determined using a 350,000 g/mol PMMA standard. These findings were subsequently used to develop a ThFFF/MALS-*d*RI method for separating and characterizing a microgel-containing PVAc sample.

3.1. PMMA standard

The manipulation of ΔT is an easy and effective way to control the separation performance and analysis time for ThFFF. Constant and programmed ΔT are used depending on the polydispersity of the sample and the desired resolution and analysis time. With programmed operation, a slow decrease in ΔT will yield better resolution but longer analysis time while the reverse is true for a rapid decrease.

Superimposed fractograms obtained using constant ΔT are shown in Fig. 2. As ΔT is increased, the peaks of both differential refractive index (*d*RI) and light scattering fractograms at 90° (I_{90}) are shifted to longer retention times and broadened. Even though separation resolution is increased with increasing field strength, the lower light scattering and *d*RI intensities associated with a broadened peak can result in the calculation of noisy and unreliable MW data such as that shown in Fig. 2B for ΔT of 55 °C. A noisy

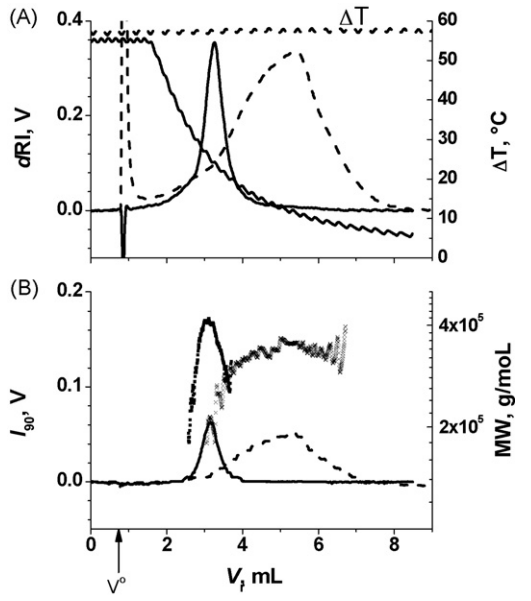

Fig. 3. ThFFF–MALS analysis of PMMA standard using constant ΔT (55 °C) and programmed ΔT (ΔT_0 = 55 °C, t_1 = 15 min, t_a = −15 min). (A) *d*RI fractograms (black line) and ΔT profiles (gray line) and (B) I_{90} fractograms and MWs. The solid and dashed lines are fractograms obtained using the programmed ΔT and constant ΔT conditions, respectively.

MW versus V_r curve was also obtained at 45 °C when the concentration of the injected sample was reduced by one-third (data not shown). This study illustrated that constant ΔT ThFFF can be used with MALS-*d*RI provided the concentration of the separated sample is sufficiently high to produce useful light scattering and *d*RI signals for calculating accurate MWs. Note also that the concentration should not be so high as to cause overloading and significant loss of separation resolution.

The use of programmed ΔT to maintain high resolution for early eluting components and accelerate elution of well retained components resulted in a noisy *d*RI signal with fluctuations that mirrored the heating cycle of the ThFFF channel's hot wall. This problem was alleviated by using a mobile phase pre-heater to regulate the temperature of the capillary tubing connecting the ThFFF channel with the MALS detector. Fig. 3 compares the results obtained using constant ΔT at 55 °C and programmed ΔT. The temperature gradient is programmed according to Eq. (1) with an initial ΔT_0 = 55 °C that is held constant for t_1 = 15 min and an asymptotic time t_a = −15 min. A shorter analysis time and narrower peaks are observed compared to constant ΔT condition.

3.2. Polyvinyl acetate sample

ThFFF/MALS-*d*RI analyses were performed on unfiltered PVAc10 and its 0.5 μm pore-size filtrate. Both fast (ΔT_0 = 55 °C, final ΔT = 5 °C, t_1 = 15 min, and t_a = −1 min) and slow (ΔT_0 = 55 °C, t_1 = 15 min, and t_a = −30 min) decay ΔTs were used in these separations. The former yielded fast analyses suitable for the early methods development stage and the latter was used in the later stage to obtain higher resolution separations.

3.2.1. Filtered PVAc10

Fig. 4A shows the *d*RI and I_{90} fractograms of the filtered PVAc10 sample and the applied ΔT profile. From the relative intensities of the *d*RI and MALS signals in different V_r regions, qualitative information can be inferred. For example, the region between 1 and 3 mL has a large *d*RI signal but low I_{90} which suggests the elution of low MW (low scattering) components while the presence of an I_{90} signal in the absence of a *d*RI signal at V_r above 5 mL is indicative of the elution of small amounts of high scattering (high MW) components. This is confirmed by MW calculations shown in Fig. 4B. Fluctuations observed near the peak maxima of both detector traces mirror those in the ΔT and do not affect the accuracy of the average molecular weights. This was verified through experiments at different concentrations and different levels of noise.

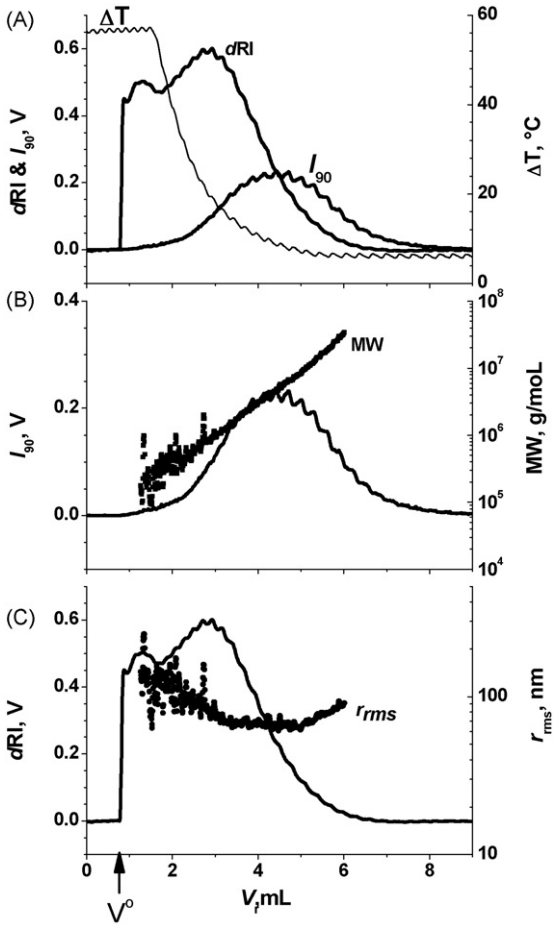

Fig. 4. ThFFF–MALS analysis of 0.5 μm pore-size filtrate of PVAc10. (A) *d*RI and I_{90} fractograms and ΔT profile, (B) I_{90} fractogram and MW and (C) *d*RI fractogram and r_{rms}. Fast-decay ΔT_0 = 55 °C, t_1 = 15 min, t_a = −1 min.

The d*n*/d*c* of the sample was estimated from the *d*RI peak area as 0.104 mL/g. The overlap of the sample peak with the solvent peak and the baseline fluctuation (see later text) caused an error in the peak area integration that was estimated from a blank run to be approximately −0.4%. The MW was calculated using 1st order Berry fitting of the scattered light intensity collected at 7 angles between 22.3° and 90.0°. The results in Fig. 4B showed the expected increase in MW (from 0.1×10^6 to 30×10^6 g/mol) as the retention volume increased (from 1.5 to 6 mL). This demonstrated the separation capability of ThFFF over a wide MW range and using a fast ΔT decay (lower resolution).

Fig. 4C shows the r_{rms} as a function of the retention volume. The r_{rms} initially decreases (between 1 and 3 mL), then holds at around 70 nm (between 3 and 5 mL), and finally increases to 90 nm (5–6 mL). In contrast to the monotonically increasing MW with increasing retention volume trend seen in Fig. 4B, the r_{rms} values exhibited a shallow U-shape trend. The r_{rms} of 90 nm at late elution volume corresponds to ultrahigh MW of 30 million g/mol, suggesting that the components eluted in this region have a highly compact structure. In other words, these component may be branched and/or crosslinked. Interestingly, the results at early elution vol-

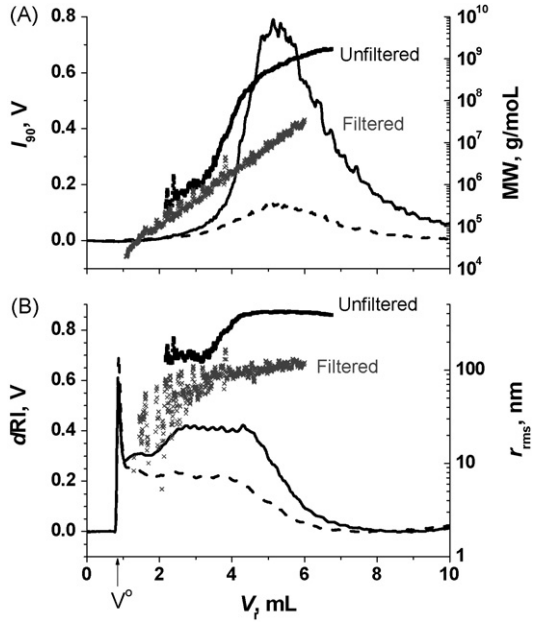

Fig. 5. ThFFF–MALS analysis of unfiltered and filtered PVAc10. 0.5 μm pore-size filter. (A) I_{90} fractograms and MWs and (B) *d*RI fractograms and r_{rms}. Solid and dashed lines represent the fractograms of unfiltered and filtered PVAc10, respectively. The black and gray lines correspond to MW or r_{rms} of the unfiltered and filtered PVAc10, respectively. ΔT is the same as that in Fig. 4.

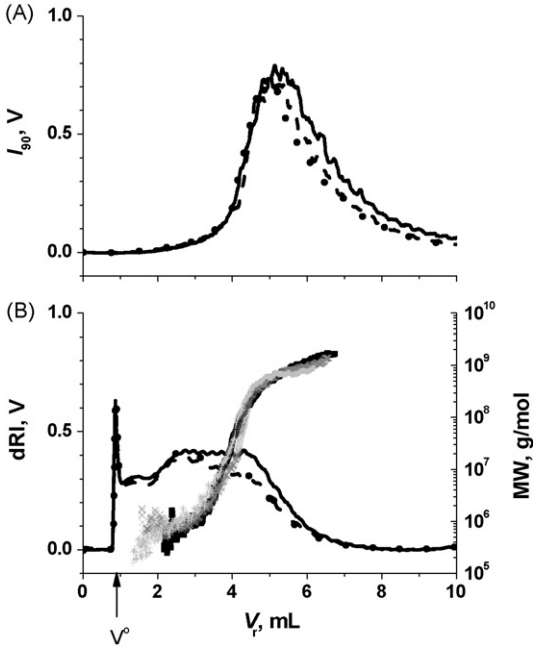

Fig. 6. ThFFF–MALS analysis of PVAc10 measured on three different days. The solid, dashed, and dotted lines represent the fractograms of one-day-old, two-day-old, and three-day-old sample, respectively. (A) I_{90} fractograms and (B) *d*RI fractograms and MWs; the black squares, gray crosses, and light-gray pluses correspond to one-day-old, two-day-old, and three-day-old sample, respectively. ΔT is the same as that in Fig. 4.

ume give the opposite observation: the r_{rms} is large (100 nm) but MW is low (200,000 g/mol). This may be due to chain entanglement caused by overloading.

3.2.2. Unfiltered PVAc10

The unfiltered and filtered PVAc10 fractograms, obtained using the fast-decay ΔT, are compared in Fig. 5. The MW of unfiltered PVAc10 was calculated using a 1st order Berry fitting of the scattered light intensity collected from 7 angles between 11.4° and 76.3°. The same d*n*/d*c* as that of filtered PVAc10 was used.

The unfiltered PVAc10 and the 0.5 μm pore-size filtrate yielded different MW and r_{rms} profiles. First, the unfiltered sample showed several distinct regions with a steep increase in MW and r_{rms} between 3.5 and 5 mL rather than the monotonic increase observed for the filtered sample. Second, the MWs and r_{rms}s of the unfiltered sample are significantly higher than those of the filtered sample. MALS-*d*RI measurements showed the presence of ultrahigh MW (~10^9 g/mol) and large (~400 nm) sample components in the unfiltered PVAc10 sample, suggestive of microgels. Further examination of the I_{90} and *d*RI fractograms revealed significant loss of polymers with MW <10^6 g/mol for the filtered sample. This is clearly evident in the different peak areas of the *d*RI fractograms.

3.2.3. Sample stability

The results of the unfiltered PVAc10 measured on three different days are shown in Fig. 6. The fractograms are slightly offset on the higher retention volume side with the one-day old sample having the highest I_{90} and *d*RI signal, followed by two- and then three-day old samples. The MW curve of the one-day old sample is also slightly higher at higher V_r. While these differences are subtle, the observed trends suggest that a larger amount of high MW sample is present in the one-day old sample and that sample dissolution should be extended beyond one day.

3.2.4. Sample recovery

The sample recovery was estimated by injecting approximately 10 mg/mL PVAc10 into the system with three different configurations. In configuration 1, tubing connections were made such that the sample was transported directly to the detector and bypassed the ThFFF channel. The sample passed through the channel with $\Delta T = 0$ in configuration 2 and passed through the channel under the slow-decay programmed ΔT in configuration 3. The *d*RI peak areas were 2.54 mL V for the run bypassing the ThFFF channel, 2.53 mL V for the run without ΔT; and 2.49 mL V for the run with the programmed ΔT. The sample recovery was estimated from relative peak areas as ~98%.

3.2.5. Slow-decay ΔT analysis

A slow-decay ΔT was used to improve the separation resolution. The parameters that describe the ΔT profile are: $\Delta T_0 = 55$ °C, $t_1 = 15$ min, and $t_a = -30$ min. Fig. 7 shows the profiles for the fast- and slow-decay ΔT programmed runs and their corresponding fractograms. As expected, the slow-decay I_{90} fractogram is shifted to a longer retention volume and is broader than the fast-decay fractogram. The lower slope of the MW–V_r plot for the slow-decay separation reflects the increase in separation resolution. The apparently higher MW at the end of the fast-decay experiment is an overestimation caused by a baseline drift in the *d*RI signal. This was confirmed by performing blank runs with acetonitrile. A downward drift was observed between 2 and 8 mL for the fast decay while a steady I_{90} baseline was evident for both fast and slow ΔT decay. These results suggested that the temperature gradient employed here did not significantly affect the light scattering signal and that blank runs should be routinely done particularly when a fast temperature program is employed.

Fig. 7B shows the *d*RI fractograms and r_{rms}s of the two different ΔT profile separations. The slow-decay *d*RI fractogram shows a distinct peak at ~2.5 mL with a long tail as the components that eluted in the plateau region of the fast-decay run are now more retained and separated. The r_{rms}–V_r plot shows a similar trend to that of the MW–V_r plot in the slow-decay ΔT separation. The MWs and r_{rms}s of the fraction eluted at 6 mL are ~4.5×10^8 g/mol and

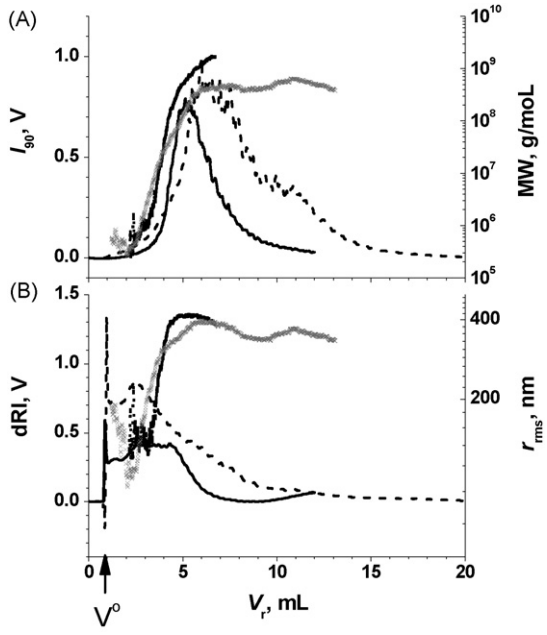

Fig. 7. Comparisons of the separations of PVAc10 using fast-decay ΔT (ΔT_0 = 55 °C, t_1 = 15 min, t_a = −15 min) and slow-decay ΔT (ΔT_0 = 55 °C, t_1 = 15 min, t_a = −30 min). The solid lines and dashed lines correspond to fractograms of fast- and slow-decay separations, respectively. (A) I_{90} fractograms and MWs and (B) *d*RI fractograms and r_{rms}.

370 nm, respectively. These should be the ultrahigh MW components corresponding to the microgels.

3.2.6. Characterization results

The characteristics of PVAc10 obtained from the slow-decay ThFFF–MALS/*d*RI analysis are the following: $M_w = 135 \times 10^6$ g/mol; M_n (number-average molecular weight) = 1.28×10^6 g/mol; PDI (polydispersity) = 105; $r_{rms,z}$ = 371 nm. The sample contained 21 wt.% of polymer with MW $\leq 4 \times 10^5$ g/mol, 23 wt.% of ultrahigh MW components with MW $\approx 4.5 \times 10^8$ g/mol, and 56 wt.% of polymer with MW in between. The obtained PDI is likely underestimated because of two reasons. (1) The low MW components eluted with the void peak are not taken into account. (2) The slow-decay ΔT has a linear fractionation power for polymers with a linear chain conformation [29] but the resolution may be insufficient for PVAc10, which has a complex polymer architecture distribution. To assure that the resolution is optimized, a higher initial ΔT should be tested to see if there is any improvement in the separation. However, this will increase the analysis time.

3.2.7. Estimation of error in MW and r_{rms}

The applicability of ThFFF to ultrahigh MW and large polymers places high demands on the MALS detector and the extrapolation techniques used as part of data treatment. MALS data analysis involves plotting some arrangement of Kc/R_θ as a function of $\sin^2(\theta/2)$. As seen in Eq. (2), extrapolating to $\sin^2(\theta/2) = 0$ (i.e., $\theta = 0°$) allows the calculation of MW from the intercept and r_{rms} from the slope [43,52]. The different ordinate axes of R_θ,/Kc, Kc/R_θ, and $\sqrt{Kc/R_\theta}$ give rise to the Debye, Zimm, and Berry plots, respectively. Each method has a different degree of curvature in the region near the *y*-intercept and thus extrapolations to $\theta = 0°$ produce different amounts of error [43]. Furthermore, Eq. (2) and its analogues are approximations based on the use of a form factor expression (Eq. (3)) applicable for high incident λ, small θ, or small scatterer size. The PVAc sample investigated in this work have large scatterers whose sizes approach the wavelength of incident light, e.g., r_{rms} = 400 nm (calculated by fitting data to Eq. (2)) and λ = 633 nm.

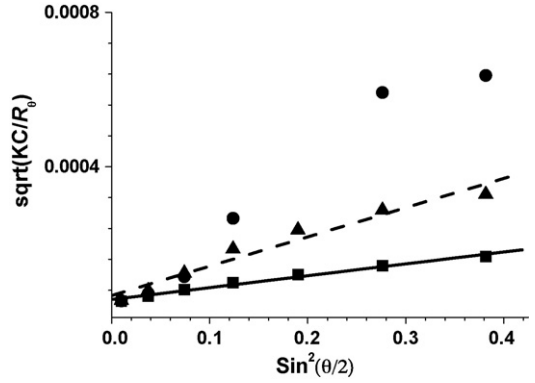

Fig. 8. Comparison of $\sqrt{Kc/R_\theta}$ versus $\sin^2(\theta/2)$ plots calculated using $P(\theta)$ expressions specific for different polymer conformations and experimentally measured results for PVAc10 at 6 mL. The squares and circles correspond to a random coil and compact sphere, respectively. A MW of 4.5×10^8 g/mol and r_{rms} of 400 nm were used in the calculations. The triangles correspond to the PVAc10 fraction.

For large scattering molecules and/or high scattering angles, $P(\theta)$ will depend on not only scattering angle and r_{rms}, but also the shape of the scatterer. $P(\theta)$ expressions have been derived for specific shapes of the scattering species and their use can provide an error estimate at these extreme conditions (MW and r_{rms}) for MALS [53,54].

Using an approach similar to that previously described in the literature [43], the scattered light intensity was calculated for a 4.50×10^8 g/mol and 400 nm sample species using $P(\theta)$ equations for random coil and compact sphere.[53,54] The calculated $\sqrt{Kc/R_\theta}$ values for θ = 11.4°, 22.3°, 31.6°, 41.2°, 51.7°, 63.4°, and 76.3° are shown in Fig. 8. The experimentally determined $\sqrt{Kc/R_\theta}$ for the PVAc fraction elution at 6 mL of the slow-decay separation is also superimposed.

The compact sphere model shows a dramatically different angular variation to the random coil and PVAc fraction. These results suggest that the conformation of this PVAc fraction is more similar to that of a random coil. The Berry formalism, when applied to the calculated data points for the random coil, yielded $M_w = 3.17 \times 10^8$ g/mol and r_{rms} = 289 nm. These values are ~30% lower than those originally used to calculate the data points. This suggests that the results calculated for the PVAc sample using the Berry formalism (Eq. (2)) are likely underestimated. It is expected that the larger the size of the sample species, the higher the underestimation.

4. Conclusions

A ThFFF–MALS-dRI method for analyzing broad polydispersity polymers with ultrahigh MW and microgels in an organic solvent has been developed. A mobile phase heater was used to thermostat the connecting tubing between the ThFFF channel and the detectors, thereby reducing fluctuations in the *d*RI signal to an acceptable level. Temperature programming can be used, but blank runs with the solvent should be done to confirm that the *d*RI signal does not drift significantly (particularly when steep ΔT gradients are used). ThFFF's ability to fractionate unfiltered sample is clearly advantageous as a more complete and accurate picture of the wide spectrum of MW and size components of a polydisperse sample is captured. Filtration of these samples prior to analysis removed the microgel components that are expected to have the most impact on rheological and other important properties. The smooth solid ThFFF walls retained all sample components within the channel and sample recoveries of ~98% were measured in the eluent. Finally, the large size of the polymers separated by ThFFF necessitated an evalu-

ation and error estimation of commonly used MALS data treatments for small scattering molecules (relative to wavelength of incident light). Using form factors specific to the shape of the scattering molecule, it was determined that the PVAc components eluting at 6 mL had more of a random coil conformation than a compact sphere and that MW and r_{rms} values determined using the standard Berry formalism were underestimated by ~30%.

Acknowledgments

The authors are grateful to ICI, National Starch and Chemical Company, NSF CHE-0515521, and NSF DMR-0820518 for financial support and samples. Dr. Tom Hahn from National Starch and Chemical Company is acknowledged for his invaluable suggestions.

References

[1] H.Y. Erbil, Vinyl Acetate Emulsion Polymerization and Copolymerization with Acrylic Monomers, CRC Press, Boca Raton, FL, 2000.
[2] L. Pille, D.H. Solomon, Macromol. Chem. Phys. 195 (1994) 2477.
[3] R. Nakamoto, R. Yasue, N.R. Gakkaishi, J. Soc. Rheol. Jpn. 31 (2003) 337.
[4] N.B. Graham, A. Cameron, Pure Appl. Chem. 70 (1998) 1271.
[5] A.F. Routh, W.B. Russel, Ind. Eng. Chem. Res. 40 (2001) 4302.
[6] D.H. Lim, H.S. Do, H.J. Kim, J. Appl. Polym. Sci. 102 (2006) 2839.
[7] D.Y. Lee, N. Subramaniam, C.M. Fellows, R.G. Gilbert, Polym. Sci. A 40 (2002) 809.
[8] I. Gonzalez, J.R. Leiza, J.M. Asua, Macromolecules 39 (2006) 5015.
[9] S. Hoefl, L. Zitzler, T. Hellweg, S. Herminghaus, F. Mugele, Polymer 48 (2007) 245.
[10] W.J. Liu, Y.M. Huang, H.L. Liu, Acta Chim. Sin. 65 (2007) 91.
[11] A. Nebioglu, M.D. Soucek, J. Polym. Sci. A: Polym. Chem. 44 (2006) 6544.
[12] V. Boyko, S. Richter, W. Burchard, K.F. Arndt, Langmuir 23 (2007) 776.
[13] X.H. Xia, Z.B. Hu, Langmuir 20 (2004) 2094.
[14] S.W. Provencher, Makromol. Chem. Macromol. Chem. Phys. 180 (1970) 201.
[15] A. Fernandez-Nieves, F.J. las Nieves, A.J. Fernandez-Barbero, Chem. Phys. 120 (2004) 374.
[16] N. Ozdemir, A. Tuncel, M.C. Kang, E.B.J. Denkbas, Nanosci. Nanotechnol. 6 (2006) 2804.
[17] A. Imaz, M. Ayerbe, J. Ramos, J. Forcada, J. Polym. Sci. A: Polym. Chem. 44 (2006) 443.
[18] H.C.M. Byrd, C.N. McEwen, Anal. Chem. 72 (2000) 4568.
[19] G.E. Kassalainen, S.K.R. Williams, Anal. Chem. 75 (2003) 1887.
[20] E.P.C. Mes, W.T. Kok, H. Poppe, R. Tijssen, J. Polym. Sci. B: Polym. Phys. 37 (1999) 593.
[21] C.S. Wu (Ed.), Handbook of Size Exclusion Chromatography and Related Techniques, 2nd ed., Marcel Dekker, New York, 2004.
[22] J.I. Ikeda, H. Oe, H. Aota, A.J. Matsumoto, Appl. Polym. Sci. 90 (2003) 577.
[23] H.G. Barth, B.E. Boyes, C. Jackson, Anal. Chem. 70 (1998) 251R.
[24] E.P.C. Mes, H. de Jonge, T. Klein, R.R. Welz, D.T. Gillespie, J. Chromatogr. A 1154 (2007) 319.
[25] G. Stegeman, A.C. van Asten, J.C. Kraak, H. Poppe, R. Tijssen, Anal. Chem. 66 (1994) 1147.
[26] G. Stegeman, R. Oostervink, J.C. Kraak, H. Poppe, J. Chromatogr. A 506 (1990) 547.
[27] J.C. Giddings, F.J.F. Yang, M.N. Myers, Science 193 (1976) 1244.
[28] J.C. Giddings, Science 260 (1993) 1456.
[29] M. Schimpf, K.D. Caldwell, J.C. Giddings (Eds.), Field-Flow Fractionation Handbook, John Wiley & Sons, New York, 2000.
[30] M.A. Benincasa, J.C. Giddings, Anal. Chem. 64 (1992) 790.
[31] J.J. Kirkland, C.H. Dilks, S.W. Rementer, Anal. Chem. 64 (1992) 1295.
[32] J.E.G.J. Wijnhoven, M.R. van Bommel, W.T. Kok, Chromatographia 42 (1996) 409.
[33] D.Y. Bang, D.Y. Shin, S. Lee, M.H. Moon, J. Chromatogr. A 1147 (2007) 200.
[34] F.A. Messaud, R.D. Sanderson, J.R. Runyon, T. Otte, H. Pasch, S.K.R. Williams, Prog. Polym. Sci. 34 (2009) 351.
[35] .J. Janca, Microthermal Field-Flow Fractionation: Analysis of Synthetic, Natural, and Biological Macromolecules and Particles, HNB Publishing, New York, 2008.
[36] S. Lee, O.S. Kwon, in: T. Provder, H.G. Barth, M.W. Urban (Eds.), Chromatographic Characterization of Polymers: Hyphenated and Multidimensional Techniques, American Chemical Society, Washington, DC, 1995, p. 93.
[37] S. Lee, J. Microcolumn Sep. 9 (1997) 281.
[38] M. Sibbald, L. Lewandowski, M. Mallamaci, E. Johnson, Macromol. Symp. 155 (2000) 213.
[39] S. Lee, C.H. Eum, A.R. Plepys, Bull. Korean Chem. Soc. 21 (2000) 69.
[40] C. Lohmann, W.G. Haseltine, J.E. Engle, S.K.R. Williams, Anal. Chim. Acta 654 (2009) 92.
[41] G.E. Kassalainen, S.K.R. Williams, J. Chromatogr. A 988 (2003) 285.
[42] B. Roda, A. Zattoni, P. Reschiglian, M.H. Moon, M. Mirasoli, M. Michelini, A. Roda, Anal. Chim. Acta 635 (2009) 135.
[43] M. Andersson, B. Wittgren, K.G. Wahlund, Anal. Chem. 73 (2001) 4852.
[44] M. Leeman, M.T. Islam, W.G. Haseltine, J. Chromatogr. A 1172 (2007) 194.
[45] E.P.C. Mes, R. Tijssen, W.T. Kok, Chromatographia 50 (1999) 45.
[46] W.S. Fulton, S.A. Groves, J. Nat. Rubber Res. 12 (1997) 154.
[47] P.S. Williams, J.C. Giddings, Anal. Chem. 59 (1987) 2038.
[48] B.H.J. Zimm, Chem. Phys. 16 (1948) 1099.
[49] G.C.J. Berry, Chem. Phys. 44 (1966) 4550.
[50] A. Gunier, Ann. Phys. 11 (1939) 161.
[51] W. Machtle, H. Fisher, Angew. Makromol. Chem. 7 (1969) 147.
[52] P.J. Wyatt, Anal. Chim. Acta 272 (1993) 1.
[53] L. Rayleigh, Proc. R. Soc. Lond. A 90 (1914) 219.
[54] P. Kratochvil, Classical Light Scattering from Polymer Solutions, Elsevier, Amsterdam, 1987.